The Budyko-Sellers Model Analysis and Determination of the Insolation Function

Panos Vlachos

April 2024

Contents

Chapter 1

Climate and The Role of EBM

Energy Blanace Models (EBM) are one-dimensional models predicting the variation of the surface temperature with latitude or the longitude. Simplified relationships are used to calculate the terms contributing to the energy balance in each latitude or longitude zone.

At the core of an EBM is the energy equation that balances incoming solar radiation with outgoing terrestrial radiation and other energy losses. The equation typically takes the form:

Internal Energy Flux Variation	=	Absorbed Energy − Reflected Energy +Diffusion

This formula is a straightforward representation of the energy fluxes entering and leaving the Earth system.

Budyko and Sellers published descriptions of models which did not depend upon the concepts already established in numerical weather prediction schemes, but attempted to simulate the essentials of the climate system in a simple way ([**10**],[**11**]). These EBMs drew upon observational data derived from descriptive climatology; for example, the reasons why the major climatic zones are roughly latitudinal. In particular, EBMs are computationally much faster than GCMs because instead of calculating the dynamical movement of the atmosphere, using the Navier–Stokes equations (as in GCMs), they employ much simpler parameterizations, and typically, much coarser grids. As a consequence of the intrinsically simpler parameterization schemes employed in EBMs, they could be applied to longer time-scale changes than the atmospheric GCMs of the time. Although the desire for longer simulation times is still an important driver for the development of simple climate model types, other demands, particularly associated with climate policy needs, are becoming increasingly important.

It was the work by Budyko and Sellers, in which the possibility of alternative stable climatic states for the Earth were identified, which prompted much of the interest in simulation of geological time-scale climatic change [**12**], and the recognition of chaos in the climate system.

1.1 Ice-Albedo Positive Feedback

Glaciers and ice caps, collectively known as the **cryosphere**, play a crucial role in regulating Earth's climate. They act as a surface feedback mechanism, particularly

sensitive to external and internal perturbations. For instance, an increase in solar luminosity or higher concentrations of atmospheric CO_2 can elevate global surface temperatures. Consequently, snow and ice melt, reducing their overall extent. These cryospheric elements possess high albedos, meaning they reflect a significant amount of solar radiation back into space. However, as their extent diminishes, less solar radiation is reflected, and more is absorbed by the Earth's surface, leading to further temperature increases. This positive feedback loop, known as the **ice-albedo feedback mechanism**, amplifies the effects of temperature changes on the cryosphere and the planet's climate system.

The concept of the ice-albedo feedback mechanism is central to the simple climate models developed by Mikhail Budyko and William Sellers. The recognition of the ice-albedo feedback mechanism as a key driver of climate change underscores the importance of understanding and accurately representing cryospheric processes in climate models and projections.

However, calculations in these models showed that if **ice extended to about 30°** latitude, one extra degree of ice cover would lead to cooling sufficient to cause one more degree of ice cover. This could lead to a **chain reaction**, eventually covering the entire Earth in ice within a few thousand years.

Despite initial skepticism, this idea is correct. At lower latitudes, one extra degree of ice cover has a greater effect because the area contained within this degree is greater, and they receive more sunlight. Thus, an increase in reflectivity at lower latitudes would be more significant than at higher latitudes, explaining why, once beyond the critical latitude, the feedback effect would only **get stronger**. Once ice cover extended that far, there would be no natural mechanism to prevent the ice sheets from reaching the Equator.

The climate instability found by scientists is now recognized as real, with concerns about the opposite extreme in which the ice cap at the Arctic and in Greenland disappears completely, causing a large rise in sea level. Once the ice cover extended that far, even a complete stop to weathering would not be sufficient to prevent a global glaciation. The mechanism required to allow an eventual thawing out from the snowball state was proposed by scientists, involving an extreme version of the carbonate-silicate cycle. Even with this mechanism, it would be very difficult to break out of such a glaciated state, requiring a level of carbon dioxide approximately **29 times higher** than its present level. The consequent rise in temperature would lead to a fairly rapid thawing of the world out of its previously frozen state. However, the actual timescale for deglaciation is not well known.

The preceding findings will be presented on the numerical analysis of the Budyko model in the next Chapters. Here is a schematic representation of the Ice-Albedo Feedback Loop:

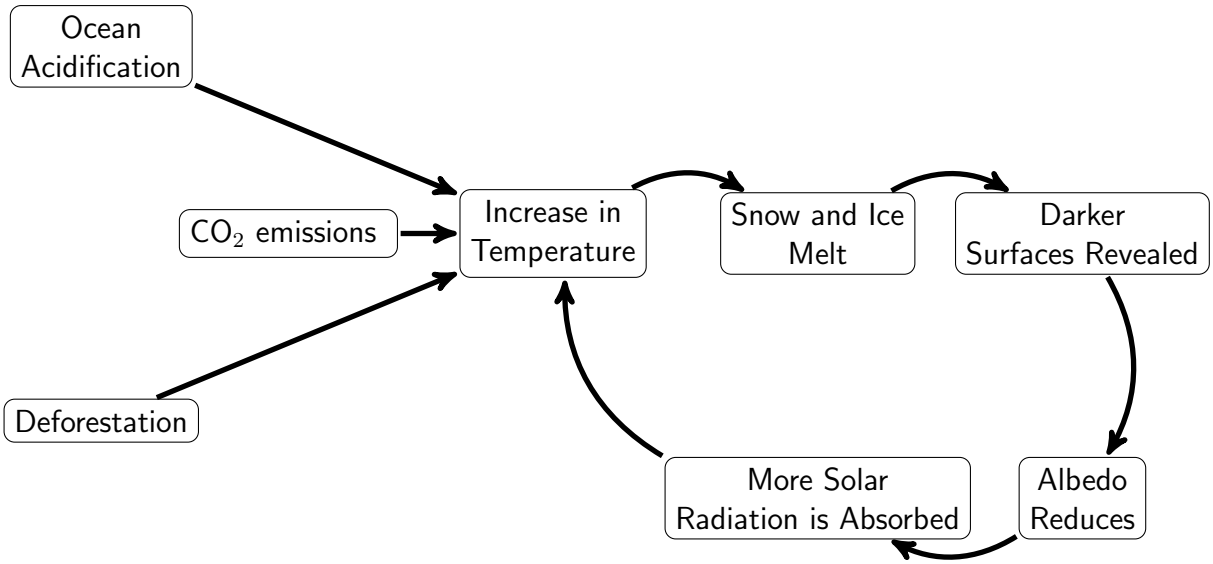

Figure 1.1: Ice-Albedo Feedback Loop with Additional Processes

1.2 Milankovitch Orbital Cycles

Milutin Milankovitch's groundbreaking hypothesis, formulated a century ago, proposed that long-term changes in Earth's orbital parameters significantly influence the planet's climate and play a pivotal role in triggering glaciation periods, commonly known as Ice Ages. His theory, now known as Milankovitch cycles, examines three primary orbital movements: eccentricity, obliquity, and precession, which collectively regulate the amount and distribution of incoming solar radiation, or insolation, at different latitudes on Earth.

Eccentricity refers to the shape of Earth's orbit around the Sun, with variations causing up to a 25 percent difference in insolation reaching Earth's mid-latitudes. Currently, Earth's eccentricity is gradually decreasing, approaching a more circular orbit over a 100,000-year cycle. Obliquity represents the tilt of Earth's axis, currently at approximately 23.4 degrees, with changes occurring over a 41,000-year cycle. Precession involves the gradual shift in the direction of Earth's axis of rotation and completes a cycle approximately every 23,000 years.

Milankovitch's calculations suggested that Ice Ages occur roughly every 41,000 years, a pattern later confirmed by research spanning one to three million years. However, around 800,000 years ago, Ice Age cycles transitioned to a 100,000-year rhythm, aligning with Earth's eccentricity cycle. Despite numerous theories proposed to explain this transition, a definitive answer remains elusive.

Initially met with skepticism, Milankovitch's work gained recognition posthumously, particularly following a 1976 study by Hays et al. that correlated Milankovitch cycles with major climate changes over the past 450,000 years, as evidenced by deep-sea sediment cores. Subsequent research, including analysis of ice cores from Greenland and Antarctica, further supported Milankovitch's theory, affirming its validity over hundreds of thousands of years.

Today, Milankovitch's theory is widely accepted within the scientific community, recognized by institutions such as the National Research Council of the U.S. National Academy of Sciences. Ongoing research continues to explore the intricate

mechanisms behind Earth's orbital variations and their specific impacts on climate dynamics, underscoring the enduring relevance of Milankovitch's pioneering work in understanding Earth's past and present climate variability.

Models addressing the seasonal cycle, like Budyko's and Seller's Models, entail more assumptions due to the introduction of time-dependence, leading to the inclusion of storage rate terms or delay terms in the energy balance equation. We will present this idea on Chapter 2.3.

1.3 Snowball Earth

The Snowball Earth hypothesis presents a fascinating and dramatic narrative in the history of our planet. First proposed by American geobiologist J.L. Kirschvink in the late 20th century, this hypothesis suggests that during two distinct periods in Earth's geological past, extreme cooling events led to the entire planet's surface being covered in ice, from the poles all the way to the Equator. These global glaciation events are thought to have occurred between 2.4 billion and 580 million years ago, marking significant and radical climate shifts in Earth's history.

Chronicle of the Snowball Earth Idea

The idea of a completely frozen Earth first gained scientific interest following the discovery of unusual geological evidence that seemed inexplicable under existing climate models. The early theories surrounding global glaciation were initially met with skepticism, as they challenged the conventional understanding of Earth's climate dynamics. However, the hypothesis gained substantial grounding through the pioneering work of Kirschvink, who meticulously analyzed geological and paleomagnetic data that supported the occurrence of these extreme glaciations.

Kirschvink's proposal was revolutionary because it offered a coherent explanation linking disparate pieces of geological data, which indicated that ice sheets extended much further toward the equator than previously believed possible during Earth's history. His hypothesis suggested that these ice sheets could have covered the entire globe, leading to a "Snowball Earth" scenario.

The Snowball Earth Hypothesis

The hypothesis asserts that Earth experienced at least two major glaciation events where ice sheets covered the land and oceans from pole to pole. This global ice cover is believed to have had profound effects on the planet's climate, atmosphere, and biosphere. Central to the hypothesis is the evidence found in ancient rock formations that not only preserved signs of Earth's magnetic field but also indicated that these rocks, associated with ice presence, were formed near the Equator—far from the polar regions where ice is typically found.

Further supporting evidence includes the discovery of a 45-metre thick layer of manganese ore in the Kalahari Desert, dated back to the end of the 2.4 billion-year Snowball Earth period. The formation of this manganese deposit is attributed to the dramatic and rapid melting of the ice, which would have triggered massive changes in ocean chemistry and global climate, leading to the deposition of minerals in concentrated layers.

In conclusion, the Snowball Earth hypothesis is underpinned by a crucial phenomenon initially identified by climate modelers using the Budyko-Sellers Energy Balance Model (EBM): the runaway ice-albedo feedback or significant ice cap instability. The Snowball Earth hypothesis not only provides a compelling explanation

for these geological phenomena but also challenges our understanding of climate dynamics and the resilience of life.

Chapter 2

The Budyko-Seller's Model

> "Essentially, all models are wrong, but some are useful.", George E. P. Box

Concerning the space variable the models are called:

1. **0D Model**: Analyzes mean Earth temperature.
2. **1D Model**: Studies mean temperature along latitudinal or vertical gradients.
3. **2D Model**: Investigates temperature distribution on Earth's surface in horizontal or meridional planes.
4. **3D Model**: General Circulation Model (GCM), considering temperature dynamics in three-dimensional space, often coupled with various Earth sciences disciplines.

2.1 2 Dimensional Model

If we conceptualize Earth as a compact two-dimensional manifold without boundary, denoted as $\mathcal{M}$, and $u(x,t)$ represents the annually or seasonally averaged surface temperature, our model can be described by a **reaction-diffusion equation**

$$c(t,x)\frac{\partial u(t,x)}{\partial t} - \operatorname{div}(k(t,x)\nabla u(t,x)) = R_a(t,x,u(t,x)) - R_e(t,x,u(t,x)) \quad (2.1.1)$$

- c(t,x): is a positive function that is frequently influenced to a significant extent by the presence of oceans. It's noteworthy that approximately 70% of Earth's surface is covered by oceans, making them a major factor in determining the overall heat capacity of the planet. Averaging $c \sim 1.05 \times 10^{23}\,\mathrm{Jm^{-2}K^{-1}}$
- the diffusion operator has a double justification:

$$\operatorname{div}(k\nabla u) = \operatorname{div}(F_c + F_a) \quad (2.1.2)$$

  with:

  - $F_c = k_c \operatorname{div} u$: the conduction heat flux
  - F_a: the advection heat flux.

- R_a: The solar energy absorbed by the Earth and it of the form:

$$R_a = SQ(t,x)\beta(u) \tag{2.1.3}$$

  where

  - S: The Solar constant, defined as the annual average amount of radiation energy per unit time passing through a unit area perpendicular to the Sun's rays at the Earth's orbit, remains consistent in our context. Averaging S$\sim 1.370 W/m^2$
  - $Q(t,x)$: The distribution of solar radiation across the Earth's surface.
  - β(u):The planetary albedo, denoted by β, represents the fraction of solar radiation absorbed by the Earth's surface, taking into account the average temperature. Typically,β is assumed to be a non-decreasing function of$u$, the surface temperature, and it maintains constant values (positive and less than 1) for any given value of$u$. In subsequent sections, we will outline the distinctions in the selection of the β function between the Budyko and Sellers models.

- $R_e(t,x,u)$: The mean emitted energy flux, denoted by R_e, represents the average energy emitted by the Earth's surface. It is empirically determined and influenced by factors such as greenhouse gases, clouds, and water vapour present in the atmosphere. Budyko's model posits a distinct value for R_e compared to Seller's model, a discrepancy that will be elaborated upon in the ensuing discussion.

The differential operators, divergence (div) and gradient (grad) must be appropriately interpreted in light of the Riemannian metric.

If we assume that $\mathcal{M}$ is the unit sphere of $\mathbb{R}^3$, the Laplace-Beltrami operator (div$(k\nabla)$) becomes:

$$\operatorname{div}(k\nabla u) = \frac{1}{\sin\phi}\{\frac{\partial}{\partial\phi}(\sin\phi\frac{\partial u}{\partial\phi}) + \frac{1}{\sin\phi}\frac{\partial^2 u}{\partial\lambda^2}\} \tag{2.1.4}$$

where ϕ is the colatitude and λ is the longitude.

2.2 1 Dimensional Model

If we take the average of the temperature at $x = \sin\phi$, which seems like a reasonable assumption (Figure 2.1), the sea level mean zonally averaged temperature $u(x,t)$ on the Earth, satisfies a quasi-linear EBM strongly degenerate problem, in the bounded domain $(-1,1)$, of the following type:

$$\begin{cases} u_t - (\rho(x)u_x)_x = R_a(x,t,u) - R_e(x,t,u), & x \in I, t > 0, \\ \rho(x)u_x = 0, & x \in \partial I, t > 0, \\ u(x,0) = u_0(x), & x \in I \end{cases} \tag{2.2.1}$$

where $I = (-1,1)$.

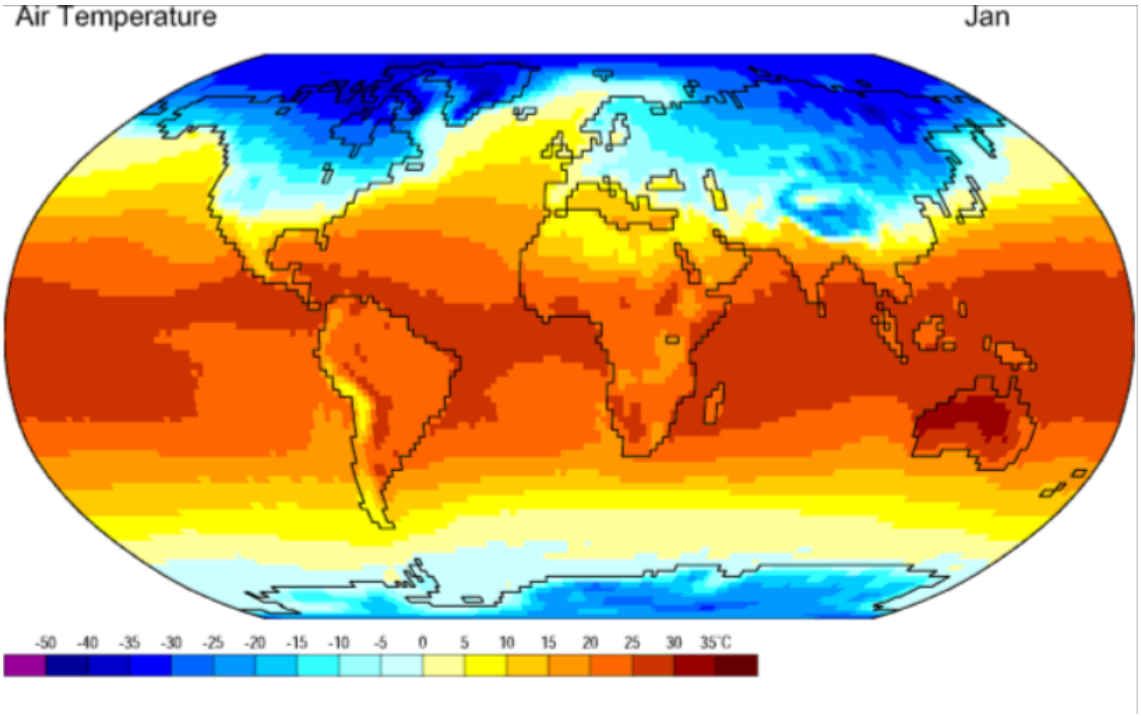

Figure 2.1: The figure shows an example of atmospheric temperature at the Earth's surface in January. Temperatures are averaged over the 1959-1997 period. Red areas correspond to a warm climate and blue areas to a cold climate.(Copyrights:https://polarpedia.eu/en/climate/)

In this work, we will make the following structural assumptions:

- $\rho(x) = k(1-x^2)$, $k > 0$
- $R_a = Q(x,t)\beta(u)$,where:
  - $Q \in C([-1,1] \times \mathbb{R}_+)$, and $Q(x,t) > 0$,
  - $\beta(u)$ is a non-decreasing and bounded function function, $|\beta(u)| \leq M$,$\forall u \in \mathbb{R}$, $M > 0$

Remark 1 *The occurrence of the degenerate diffusion term* $(1-x^2)$ *comes from the transformation* $x = \sin\phi$ *and the equation (2.1.1)*

According to the above assumption, one has the following reaction-diffusion equation with reflecting Boundary Conditions:

$$\begin{cases} u_t - ((1-x^2)u_x)_x = Q(x,t)\beta(u) - R_e(x,t,u), & x \in I, t > 0, \\ (1-x^2)u_x = 0, & x \in \partial I, t > 0, \\ u(x,0) = u_0(x) \end{cases} \tag{2.2.2}$$

We have not yet made any assumptions about the function R_e, which represents the energy emitted by the Earth. The value of R_e might be influenced by various factors such as the concentration of greenhouse gases, the presence of clouds and water vapor in the atmosphere, and changes caused by human activities.

Next, we will explore the key differences between the Budyko and Seller models. While both models incorporate similar elements like the diffusion term and the

Incoming Solar function, there are distinct assumptions in each model that we'll outline.

For the **Incoming Solar Flux** we assume $Q(t,x) = q(x)r(t)$ where q is the **insolation function** and:

$$\begin{cases} q \in L^\infty(I) \\ r \in C^1(\mathbb{R}_+) \text{ and } r, r' \in L^\infty(\mathbb{R}_+) \end{cases} \tag{2.2.3}$$

The **Budyko type coalbedo** function is given by the form:

$$\beta(u) = \begin{cases} a_i, & u < -10°C \\ [a_i, a_f], & u = -10°C \\ a_f, & u > -10°C \end{cases} \tag{2.2.4}$$

In contrast, the **Seller's type coalbedo** is taken as:

$$\beta \in C^2(\mathbb{R}) \quad \text{and} \quad \beta, \beta', \beta'' \in L^\infty(\mathbb{R}) \tag{2.2.5}$$

Additionally, both models define the function R_e, which represents the energy emitted by the Earth. In Budyko's model, this radiation function, R_e, is assumed to be a linear function of temperature:

$$R_e(u) := a + bu, \quad s \in \mathbb{R} \quad \text{and} \quad b > 0 \tag{2.2.6}$$

In contrast, in Seller's work the radiation function emitted by the Earth follows a Stephan-Boltzmann type law:

$$R_e(u) := \epsilon(u)|u|^3 u \tag{2.2.7}$$

meaning that the Earth radiates as a black-body. In the formula (2.2.7), $\epsilon(u)$ denotes the **emissivity** and is a positive bounded function taken as:

$$\epsilon(u) := \sigma\big(1 - m\tanh\big(\frac{19u^6}{10^6}\big)\big)$$

where $\sigma > 0$ represents the **emissivity coefficient** and $m > 0$ indicates the **atmospheric opacity**.

Remark 2 *Notice that equation (2.2.6) corresponds to a linear approximation of (2.2.7) near the actual mean temperature of 15°C.*

Remark 3 *A draw-back of the model, occurs in this step and is related to the direct linkage of albedo and temperature, which neglects completely the long response times of the continental ice-sheets.*

We are now able to write the most general form of the two models, in Budyko's and Seller's case.

Seller's Model

$$\begin{cases} u_t - ((1-x^2)u_x)_x = r(t)q(x)\beta(u) - \varepsilon(u)|u|^3 u, & x \in I, t > 0, \\ (1-x^2)u_x = 0, & x \in \partial I, t > 0, \\ u(x,0) = u_0(x) \end{cases} \tag{2.2.8}$$

Budyko's Model

$$\begin{cases} u_t - ((1-x^2)u_x)_x = r(t)q(x)\beta(u) - \alpha + bu, & x \in I, t > 0, \\ (1-x^2)u_x = 0, & x \in \partial I, t > 0, \\ u(x,0) = u_0(x) \end{cases} \tag{2.2.9}$$

2.3 The EBM with Memory(EBMM) model

In a notable extension of reaction-diffusion Energy Balance Models (EBMs), a delay mechanism was introduced to address the prolonged response times of ice sheets to temperature fluctuations. This innovative approach, outlined in [**7**], incorporates a memory function within the albedo parameterization, allowing past temperatures to influence the present albedo and consequently modify shortwave radiation terms.

This augmentation acknowledges the temporal lag between temperature changes and the corresponding response of ice sheets, a critical aspect often overlooked in traditional EBMs. By integrating historical temperature data into the albedo function, the model more accurately captures the dynamics of ice-albedo feedback and the associated impact on shortwave radiation balance.

This advancement not only enhances the realism of EBMs but also opens avenues for exploring the complex interplay between climate variables over extended time scales. Through the integration of memory mechanisms, EBMs can better simulate the nonlinear dynamics inherent in Earth's climate system, providing valuable insights into long-term climate variability and feedback mechanisms.

Let's now formalize this history term that will advance the dynamics of the EBM. To do this we will introduce a **history function** that takes the form:

$$H(t,x,u) = \int_{-\tau}^{0} \kappa(s,x)u(s+\tau,x)\,ds \tag{2.3.1}$$

where κ is the kernel term with the followign properties:

- $\kappa(\cdot,s) > 0, \quad s \in (-T,0)$
- $\kappa(\cdot,-T) = 0$
- $\int_{-T}^{0} \kappa(\cdot,s)\,ds = 1$
- $\kappa \in C^1([-\tau,0]\times[-1,1];\mathbb{R})$

Remark 4 *When we will study the Inverse Problem for the EBMM we will consider an additional property of the kernel κ that reads:*

$$\exists \epsilon > 0 \quad \textit{such that} \quad \kappa(s,\cdot) = 0, \qquad [-\epsilon,0] \tag{2.3.2}$$

The system (2.2.1) becomes:

$$\begin{cases} u_t - (\rho(x)u_x)_x = R_a(x,t,u) - R_e(x,t,u) + f(H), & x \in I, t > 0, \\ \rho(x)u_x = 0, & x \in \partial I, t > 0, \\ u(x,0) = u_0(x) \end{cases} \tag{2.3.3}$$

where f introduces the memory effect in the system. We assume that:

- $f : \mathbb{R} \to \mathbb{R}$ and $f \in C^1$
- $f, f' \in L^\infty(\mathbb{R})$
- f, f' are Lipschitz functions

Since $H(t,x,u)$ is defined for a past temperature, we have to change the initial condition and substitute it by the following one:

$$u(s,x) = u_0(s,x), \qquad \text{for all } \; s \in [-\tau,0], \quad x \in I \tag{2.3.4}$$

We will further explain the purpose behind this choice on the next Chapters.

Chapter 3

Well Possedness

3.1 Well Possedness of EBM

In this section, we'll establish the functional framework guiding our analysis. Due to the degeneracy of the diffusion term, we'll employ weighted Sobolev spaces, offering an effective treatment for this particular scenario.

Set:

$$Y = \{y \in L^2(I) : \sqrt{\rho} y_x \in L^2(I)\} \tag{3.1.1}$$

As we have already stated, set I denotes the interval $(-1, 1)$.

The associated inner product and the corresponding norm are as follows:

$$(u, y)_Y := (u, y)_{L^2(I)} + (\sqrt{\rho} u_x, \sqrt{\rho} y_x)_{L^2(I)} \tag{3.1.2}$$

and

$$\|u\|_Y := \sqrt{(u, y)_Y} \tag{3.1.3}$$

We aim to recast our system (2.2.2) into the evolution equation:

$$\begin{cases} u_t(t) + Au(t) = P(t, u(t)), & t \in [0, T] \\ u(0) = u_0 \end{cases} \tag{3.1.4}$$

To do so, we introduce the following degenerate diffusion operator:

$$\begin{cases} D(A) := \{u \in Y | v \mapsto \int_{-1}^{1} a(x) u_x v_x \, dx \text{ is } L^2(I) \text{ continuous}\} \\ \forall u \in D(A), \forall v \in V, \quad (Au, v) = \int_{-1}^{1} a(x) u_x v_x \, dx \end{cases} \tag{3.1.5}$$

Then one has the following characterization of the operator A:

Theorem 1 *Operator $(A, D(A))$ is the infinitesimal generator of an analytic semigroup $S(t)$.*

Proof: Notice that $\exists \gamma > 0$ and $\theta \in \mathbb{R}$ such that for every u:

$$\int_{-1}^{1} a(x)(u_x)^2 \, dx + \gamma \|u\| + L^2(I)^2 \geq \theta \|u\|_V^2 \tag{3.1.6}$$

By directly applying Theorem 2.12[**15**,p.115] , we obtain the required result, thereby completing the proof.

□

Lemma 1 *The couple* $(A, D(A))$ *satisfies:*

$$\begin{cases} D(A) := \{u \in Y | \rho u_x \in H^1(I)\} \\ \forall u \in D(A), Au := -(\rho u_x)_x \end{cases} \tag{3.1.7}$$

From the above definition, we deduce that the operator A is unbounded, represented by: $A : D(A) \subset L^2(I) \to L^2(I)$.

It is well known that the above operator generates an analytic semigroup, e^{At}[**2**]. Therefore, the system below is well-defined and admits a unique solution on I:

$$\begin{cases} u_t + Au = 0, & x \in I, t > 0 \\ u(x, 0) = u_0(x) \end{cases} \tag{3.1.8}$$

Remark 5 *Notice here that (3.1.8) we haven't included a boundary condition. That is because of the structure of the space* $D(A)$*, where the condition* $(\rho u_x)_x \in L^2(I)$ *implies that* u *satisfies* $(\rho u_x)(x) = 0$ *on* ∂I*.*

The statement above can be easily proven using the method of contradiction. Let's walk through the proof.

Given that ρu_x belongs to $H^1(I)$, it implies that ρu_x is in $C^0([-1, 1])$. Let's assume that as x approaches -1, $|\rho u_x|$ tends to L, where $L > 0$. Then, there exists a region close to $x = -1$ where $|\rho u_x| \geq L/2$. By rearranging the inequality, we get $|\sqrt{\rho} u_x| \geq \frac{L}{2\sqrt{\rho}}$. This contradicts the fact that $\sqrt{\rho} u_x$ is in $L^2(I)$, since $\frac{1}{\rho} \notin L^1(I)$. Hence, we conclude that $L = 0$.

By following the same procedure, it can be demonstrated that $\rho u_x(1) = 0$.

We define the function P on the $L^2(I)$ space:

$$\forall t \in [0, T], u \in Y \qquad P(x, u(t)) := r(t) q \beta(u) - \varepsilon(u)|u|^3 u \tag{3.1.9}$$

Notice that the function is well-defined. Then the following system:

$$\begin{cases} u_t(t) + Au(t) = P(t, u(t)), & t \in [0, T] \\ u(0) = u_0 \end{cases} \tag{3.1.10}$$

is a recast of (2.2.2), and is well-possed by a perturbation argument.

In this work, we will focus on the global existence of the regular solution, and we will try to avoid some technical steps that one has to follow to deal with the well-posedness of the solution.

We define the restricted set of initial conditions:

$$\mathcal{U} := \{u_0 \in D(A) \cap L^\infty(I) : Au_0 \in L^\infty(I)\} \tag{3.1.11}$$

Theorem 2 *Let* $u_0 \in \mathcal{U}$*. Then the solution* u *of (2.2.2) is defined on the interval* $[0, \infty)$*.*

Remark 6 *Theorem 2 ensures that the solution* u *does not blow up at any time* $t \in [0, \infty]$ *and the the following inequalities are satisfied:*

1. $\|u\|_Y < \infty$

2. $\|u\|_{L^\infty((0,T)\times I)} < \infty$

A schematic diagram illustrating the process we followed, is presented below.

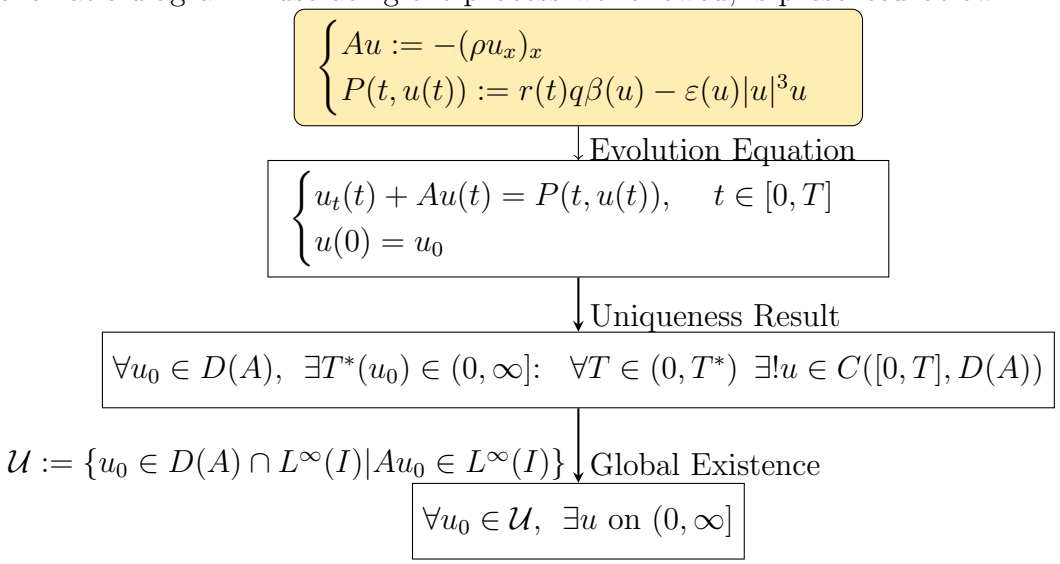

3.2 Well Possedness of EBMM

The functional set up for this EBMM is similar with the one presented on the previous section (EBM) and we will omit some steps. We will try to briefly introduce the functional framework and briefly give two existence theorems related to the EBMM corresponding to the Seller's and Budyko's models.

For the case of the EBMM we introduce the following weighted Sobolev space:

$$Y := \{y \in L^2(I) : y \in AC_{loc}(I),\ \sqrt{\rho} y_x \in L^2(I)\} \tag{3.2.1}$$

where AC denotes the class of Absolutely Continuous functions.

We will use the norms and the operators that has been used on the previous section. Here are some differences from the previous model:

Introduce the **Right Translation**:

- $u_t \in C([-\tau, 0] \to L^2(I))$ a continuous mapping
- $u_t(s) := u(t+s), \qquad u \in C([-\tau, T]; L^2(I))$

and let's also define:

$$\begin{cases} J : C(-\tau, 0); L^2(I) \\ J(w)(x) := f(H(w)) \end{cases} \tag{3.2.2}$$

Then the evolution equation (3.1.10) is substituted by the following:

$$\begin{cases} u_t(t) + Au(t) = P(t,u(t)) + J(u_t), \quad t \in [0,T] \\ u(s) = u_0(s), \forall s \in [-\tau, 0] \end{cases} \tag{3.2.3}$$

It is necessary to give a definition related to the nature of the solution for the particular problem.

Definition 1 *Given the initial condition $w_0 \in C([-\tau, 0]; Y)$ a function:*

$$w \in H^1(0, T; L^2(I)) \cap L^2(0, T; D(A)) \cap C([-\tau, T]; Y) \tag{3.2.4}$$

is **mild solution** of 3.2.3 if

1. $w(s) = w_0(s), \quad s \in [-\tau, 0]$
2. $\forall t \in [0, T]$:

$$w(t) := e^{At} w_0(0) + \int_0^t e^{(t-s)A}(P(s, w) + J(w_t))\, ds \tag{3.2.5}$$

where w_t is the right translation.

We are ready to present the existence theorems for both models:

Theorem 3 *Suppose that $u_0 \in C([-\tau, 0]; Y)$ and $u_0(0) \in D(A) \cap L^\infty(I)$*

then:

1. For the Seller's model: for $T > 0$ the system (3.2.3) admits a unique mild solution on $[0, T]$.
2. For the Budyko's model: the system (3.2.3) has a mild solution, which is global in time. $(T = \infty)$

Chapter 4

Numerical Results

In this chapter, we will present numerical results for the Budyko-type model. To ensure that our model is both reasonable and realistic, we will carefully adjust the parameters to reflect current behaviors. Below, we describe the model configuration that we will simulate.

$$c\frac{\partial u}{\partial t} - \frac{D}{\sin\phi}\frac{\partial}{\partial\phi}(\sin\phi\frac{\partial u}{\partial\phi}) = (1-\alpha)Q - (a+bu) \tag{4.0.1}$$

where we have chosen:

- $a = 210\ Wm^{-2}$, is the emission at $0°C$
- $b = 2\ Wm^{-2}\ °\mathrm{C}^{-1}$, rise in emissions per degree, associated with the net long-wave climate feedback.
- $D = 0.55\ Wm^{-2}\ °\mathrm{C}^{-1}$, constant diffusivity of the system
- $Q = \overline{Q(\phi)}$, annual mean insolation.
- $\alpha(\phi) = \alpha(\phi, u(\phi)) = \begin{cases} \alpha_0 + \alpha_2 P_2(\sin\phi), & u(\phi) \geq -10°C \text{ (no ice)} \\ \alpha_i, & u(\phi) < -10°C \text{ (ice covered)} \end{cases}$ is the albedo function and we made the additional adjustment:
  - $\alpha_0 = 0.3$
  - $\alpha_2 = 0.078$
  - $\alpha_i = 0.62$
  - $P_2(\phi) = \frac{1}{2}(3\phi^2 - 1)$ is the Legander Polynomial

Here, we operate under the assumption that in areas where temperatures exceed $-10°C$, ice cover cannot form. Consequently, if the temperature satisfies $u(\phi) > -10°C$ for all $\phi \in [-90, 90]$, it implies a scenario where the Earth is completely devoid of ice-covered regions. Conversely, if $u(\phi) \leq -10°C$ for all $\phi \in [-90, 90]$, it indicates a Snowball Earth scenario, where the planet is entirely encased in ice.

The selection of the diffusion coefficient D carefully considers the pole-to-equator temperature gradient and peak poleward heat transport and is sophisticatedly chosen to study the behavior of temperature under varying solar radiation conditions.

For our analysis, we will use a Python package called "Climlab". I give the credits in the following lines:

Credits The Python package is part of The Climate Laboratory, an open-source textbook developed and maintained by Brian E. J. Rose, University at Albany.

4.1 Consistency of the Model

Running the model for the assumed (default) values we get the following figures

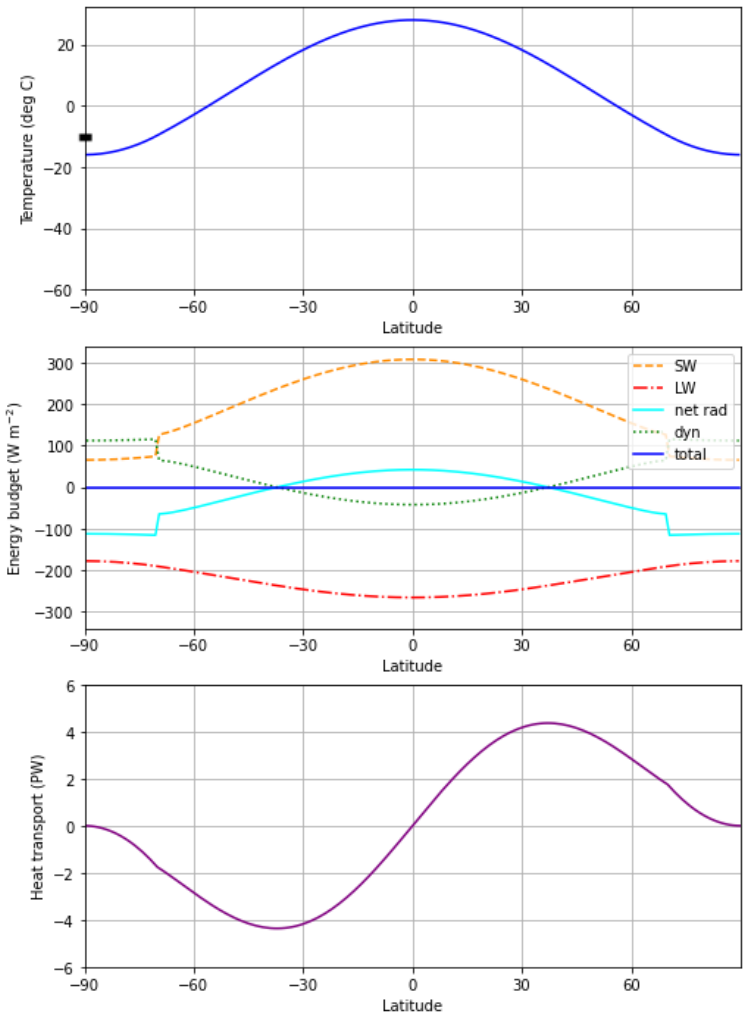

Figure 4.1: Energy Balance

In the upper figure, we present the annual distribution of global temperatures across different latitudinal belts. This distribution effectively captures a realistic view of the Earth's current climate, showcasing satisfactory model performance.

Additionally, the model accurately identifies the current location of the ice edges within the latitudinal zones of $[-90, -70]$ and $[70, 90]$, providing a robust approximation. It is crucial to note the symmetric behavior of the system, particularly the mild delineation at the Earth's equator, which further enhances our understanding of global climatic patterns.

The other two figures illustrate the behavior of the model concerning energy dynamics. Specifically, the middle figure demonstrates that the multifactorial system

maintains a total Energy Budget of zero, affirming the appropriateness of using the term Energy Balance Model (EBM).

The final figure displays the Heat Transport across different latitudes. Notably, the minimum points occur at the poles and the Equator, indicating a lack of energy transport at these locations. Conversely, the maximum values are observed around ± 40 degrees latitude, suggesting that these regions are pivotal in driving the heating process.

4.2 Tuning the Emissivity Function

In the previous Section we concluded that the studying system with the default parameters is consistent, as it reflect the real picture of the annual zonal temperature. It would be interested to see how the system behaves if we tune in a different way some of the parameters. We will start by changing the values of the emission function: $R_e := a + bu$.

The most important parameter seems to be the emissivity a. Here we present some results of tuning this parameter.

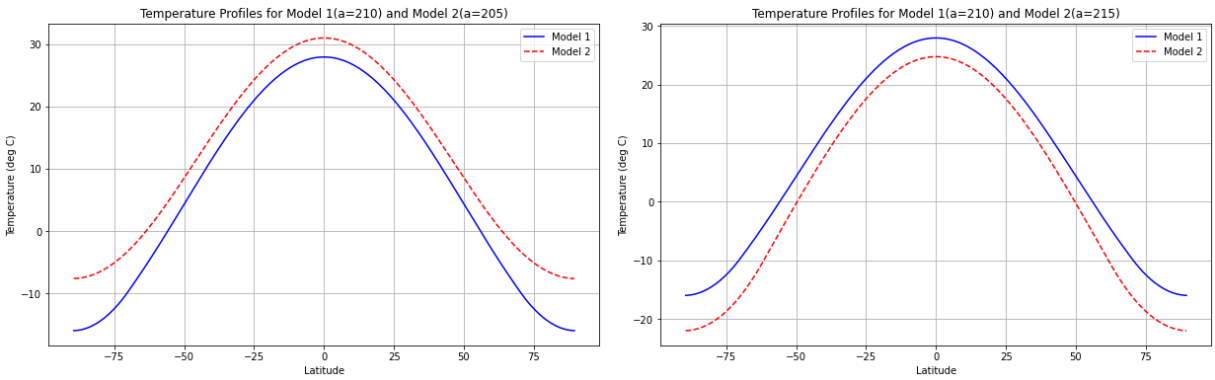

(a) Run 1 (b) Run 2

Figure 4.2: The Impact of Minor Adjustments on the Parameter a—Emission Function

It is evident that even a slight modification to parameter a can have significant consequences for Earth's climate. The temperature profile above illustrates that a reduction of 5 in parameter a could result in a complete melting of the ice caps, consequently leaving the planet without any ice lines, as indicated by $u \geq 10$.

Therefore, the model suggests that our planet is highly sensitive even to minor changes in emissivity, which can significantly influence global climate dynamics. Even small variations in emissivity could potentially lead to substantial global warming, highlighting the delicate balance of Earth's atmospheric conditions and the critical importance of monitoring and managing these parameters to mitigate adverse climate impacts.

It would be an interesting experiment to check for which values of the parameter a, and without changing the other ones, an Snowball Earth can occur. By choosing $a = 233.85$ we get the following Temperature Profil:

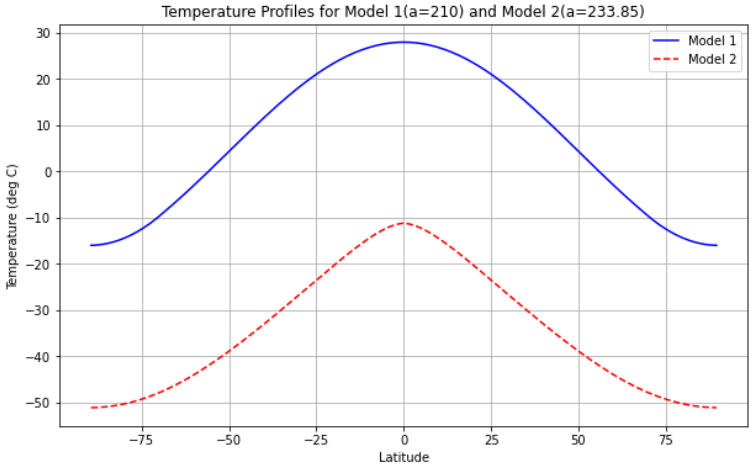

Figure 4.3: Adjusting the Parameter a-Emission Function to Induce a Snowball Earth Scenario

As observed, the peak temperature in the Model's 2 Temperature Profile occurs at $-10°C$indicating that even the warmest temperatures are at the freezing point, resembling conditions of a frozen Equator. Consequently, setting the value of$a$ to 233.85 or higher results in a Snowball Earth scenario, where the entire planet is enveloped in ice.

4.3 Tuning the Insolation Constant

In this section, we will maintain all parameters at their default settings while exploring the model's response to different values of solar radiation, Q. It is logically sound to anticipate that increasing the insolation constant would lead to a rise in temperature. Conversely, reducing the insolation constant would have the opposite effect, leading to a decrease in temperature. This analysis will help us understand the direct impact of solar radiation on Earth's climate according to the model.

The model takes as a default insolation constant the value: $1365.2Wm^{-2}$. We reduce the insolation constant by $\approx 5\%(1290Wm^{-2})$, and we get the following diagram:

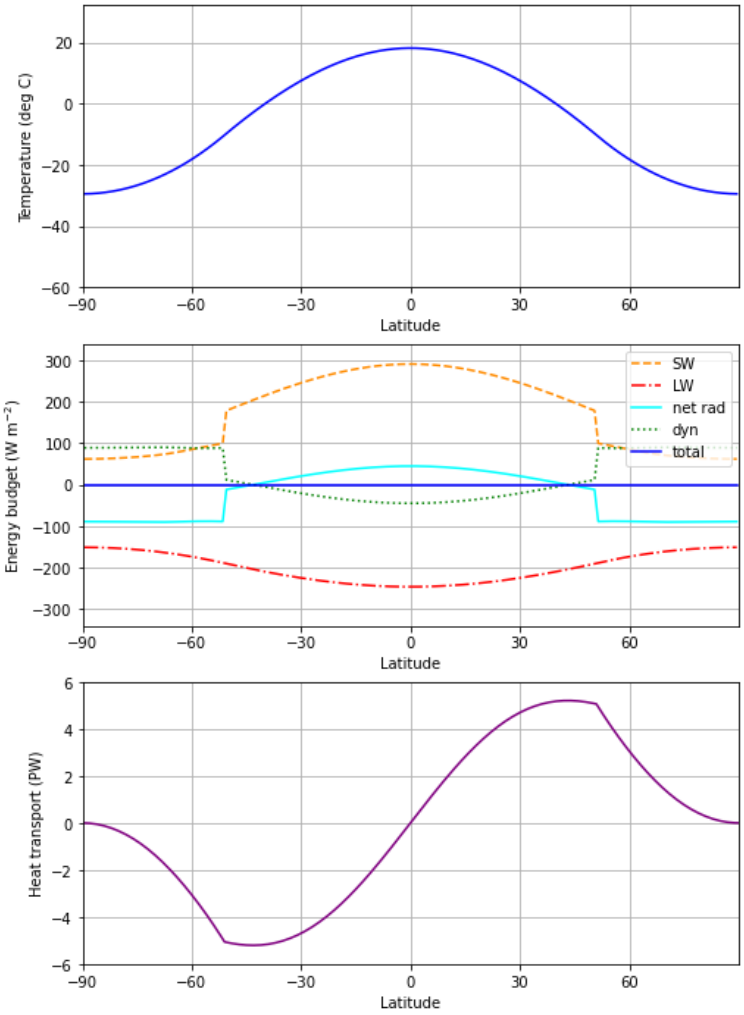

Figure 4.4: Insolation Constant $Q = 1290\ Wm^{-2}$

Our qualitative prediction has been validated, as evidenced by the effects of reducing the insolation constant, which resulted in a colder climate. This change led to a noticeable shift in the ice line, now extending closer to the equator, covering latitudes from $[-90, -51]$ to $[51, 90]$. This movement of the ice line toward the equator reflects the substantial impact that solar radiation has on Earth's temperature distribution and climatic conditions. The experiment underscores the sensitivity of Earth's climate system to variations in solar insolation, providing a clear demonstration of how changes in external energy inputs can shift climatic zones and alter global temperature patterns.

Additionally, the last figure, which illustrates the Heat Transport, indicates a significant shift towards the poles, suggesting that the majority of heat transport now occurs at the latitudes of $\pm 50°C$. This observation underscores a redistribution of thermal energy across the globe, with enhanced movement of heat towards higher latitudes, potentially due to changes in atmospheric and oceanic circulation patterns triggered by the altered climate conditions.

4.3.1 Bistability Result-Snowball Earth

Let's further reduce the insolation constant to the value $1210°C$ and observe the outcome of the model. This adjustment is expected to significantly impact the model's temperature profiles and heat transport mechanisms, potentially intensifying the cooling effect and altering the climatic conditions even more drastically.

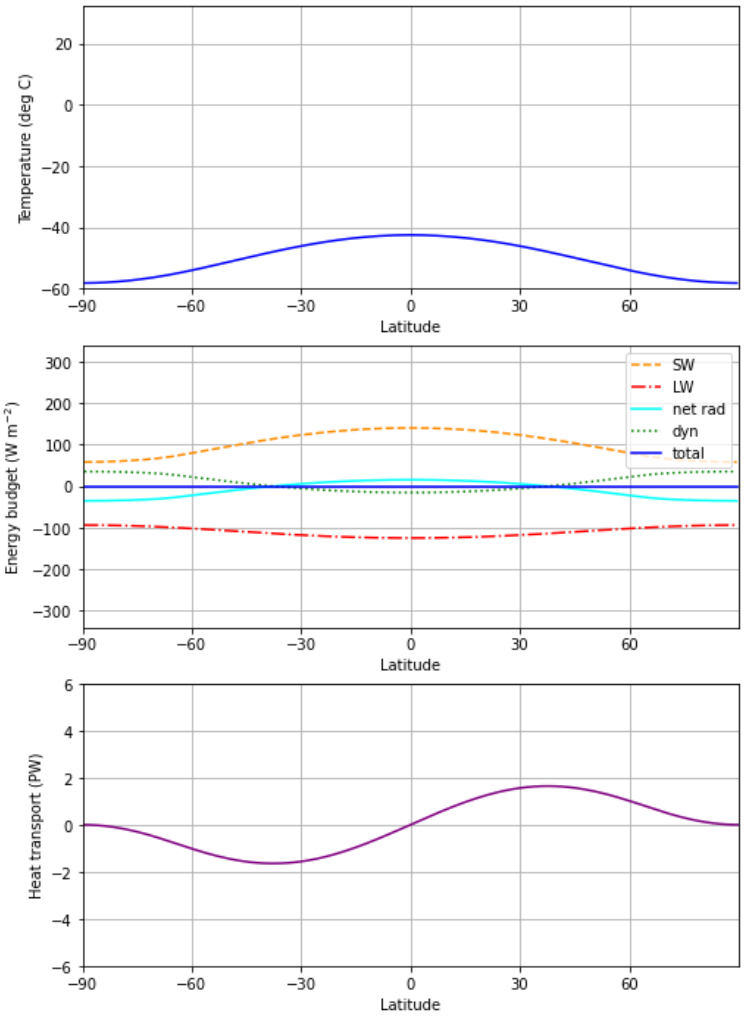

Figure 4.5: Insolation Constant $Q = 1210\ Wm^{-2}$

Now, we observe that we have indeed achieved a Snowball Earth scenario, with the highest recorded temperature around $-40°C$ There is minimal interaction between neighboring areas as heat transport has been dramatically reduced, resulting in a uniformly frozen climate. This severe limitation in thermal exchange across different regions leads to a static environment with very limited dynamic atmospheric activity. This outcome highlights the profound impact that significant reductions in solar radiation can have on Earth's climate system.

If we reset the insolation constant back to its default value of $(1365.2Wm^{-2})$, the resulting Temperature Profile is depicted in the figure below:

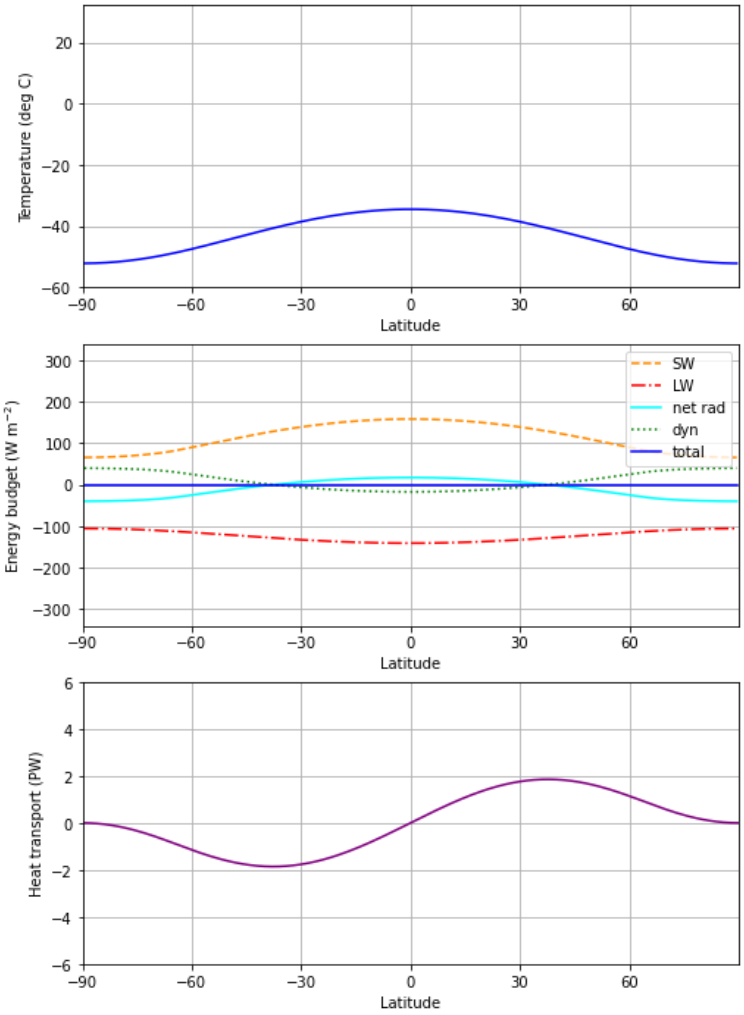

Figure 4.6: Tuning back the Insolation Constant $Q = 1365.2\ Wm^{-2}$-Hysteresis

From the figure, it is evident that while the temperature has increased by almost $10°C$, the general behavior of the climate system remains substantially unchanged. This minimal response highlights the inertia inherent within the climate system once it has transitioned into a stable state.

This phenomenon of minimal change despite significant alterations in solar radiation can be attributed to hysteresis. **Hysteresis** occurs when a system stabilizes in a new state—such as the Snowball Earth scenario observed here—and exhibits resistance to returning to its original state. This resistance is a critical feature of many natural systems, demonstrating their ability to latch onto new equilibria.

The persistence of the Snowball Earth condition, despite returning to the original insolation levels, emphasizes the complexity and resilience of Earth's climate system. It illustrates how drastic climatic shifts, once set in motion, can create new stable states that are difficult to reverse, underscoring the importance of understanding and managing our environmental interventions to avoid irreversible changes.

We are set to examine the dependency of the equilibrium ice edge on the solar constant Q by systematically adjusting Q in our model and observing its approach to equilibrium at various levels. Initially, we will gradually decrease Q, and then slowly increase it, exploring up to three distinct climatic states that may exist for a given Q. Here is the required figure:

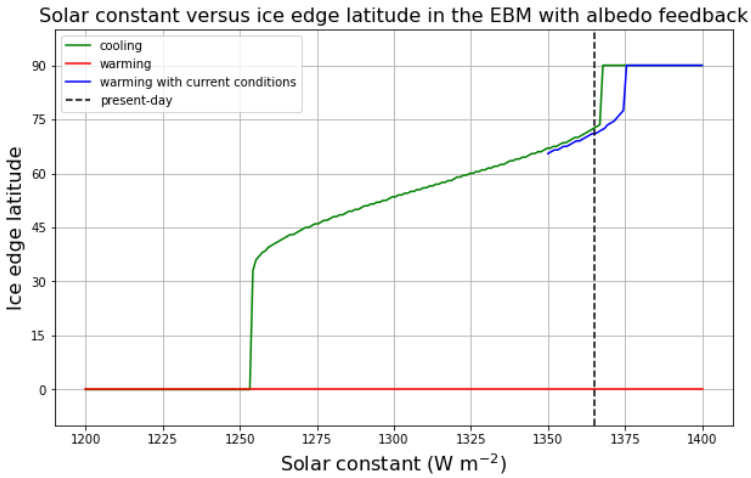

In this figure, we observe at least two stable climates, represented by the red and green lines. It is particularly noteworthy to observe the abrupt transition at $Q = 1253$, here the ice edge latitude jumps from 35° to the Equator. This behavior is attributed to the discontinuities, or "jump terms," inherent in the Energy Balance Model (EBM).

Additionally, a second critical transition occurs near the current value of the solar constant. This indicates that a slight increase in the solar constant could result in the complete disappearance of the ice caps. This finding highlights the delicate balance maintained by Earth's climate system and the significant impact of solar radiation on ice cover stability.

Chapter 5

Determination of the Insolation Function

5.1 The Inverse Problem and Lipschitz Stability for the Seller's EBM

The work of Tort and Vancostenoble [**8**] provides a general method of dealing with a wide class of inverse problems of non-linear parabolic PDEs. In our case, they try to find the unknown coefficient in a non-linear term in the 1D Sellers climate model, by establishing an unconditional global Lipschitz stability. By doing this, we get in addition a uniqueness result, meaning that for every solution u of the PDE system corresponds a unique insolation function q.

In order to deal with the Lipschitz stability we define the **set of admissible coefficients**:

$$\mathcal{G}_K := \{q \in L^\infty(I) : \|q\|_{L^\infty(I)} \leq K\} \tag{5.1.1}$$

The Inverse Problem refers to the question:

■ Is it possible to recover the insolation function **q** from some measurements of the temperature u?

This question can be expressed in mathematical terms as:

■ Suppose we have two functions: u and $\tilde{u}$ and the associated insolation functions of its temperature are q and $\tilde{q}$. Then if these quantities satisfy the following systems:

$$\begin{cases} u_t - ((1-x^2)u_x)_x = r(t)q(x)\beta(u) - \varepsilon(u)|u|^3 u, & x \in I, t > 0, \\ (1-x^2)u_x = 0, & x \in \partial I, t > 0, \\ u(x,0) = u_0(x) \end{cases}$$

$$\begin{cases} \tilde{u}_t - ((1-x^2)\tilde{u}_x)_x = r(t)\tilde{q}(x)\beta(\tilde{u}) - \varepsilon(\tilde{u})|\tilde{u}|^3 \tilde{u}, & x \in I, t > 0, \\ (1-x^2)\tilde{u}_x = 0, & x \in \partial I, t > 0, \\ \tilde{u}(x,0) = \tilde{u}_0(x) \end{cases}$$

can one deduce the following expression:

$$u = \tilde{u} \text{ in a small set } \implies q = \tilde{q} \text{ in a small set?} \tag{5.1.2}$$

The following theorem states the Lipschitz stability.

Theorem 4 *Let $t_0 \in (0,T)$ be given and consider the time:*

$$T^* := \frac{T+t_0}{2}$$

Let $\phi \in (L_1, L_2)$ where $L_1, L_2 \in (-1,1)$ and $L_1 < L_2$. If $u \in \mathcal{U}$, then for all $K > 0$ $\exists D > 0$ such that, for all $q_1, q_2 \in \mathcal{G}_K$, the associated solutions u_1, u_2 of problem (2.2.2) satisfy:

$$\|q_1 - q_2\|_{L^2(I)} \leq D\Big(\|(u_1-u_2)(T^*,\cdot)\|^2_{D(A)} + \|u_{1,t} - u_{2,t}\|^2_{L^2((t_0,T)\times\phi)}\Big) \tag{5.1.3}$$

The proof of this theorem is based on the use of global Carleman estimates for parabolic problems, an advanced energy estimation method. In this work we will omit the derivation of this theorem due to the technical difficulties occurred. Our stability can be understood unconditional in the sense that we do not need to assume any a priori boundedness conditions.

5.2 The Inverse Problem and Lipschitz Stability for the EBMM

The Inverse Problem for the Seller's type Energy Balance Model with Memory was explored by Cannarsa et al. (2018) in [**9**]. This study builds upon the work presented in the previous section, which focused on the paper [**8**]. The authors examined two distinct inverse problems, differing primarily in their assumptions about the control region. Specifically, unlike the earlier results where we assumed the control region to be $\mathcal{U}$, this work introduces two different scenarios characterized by distinct sets of **admissible initial conditions** and **admissible coefficients**:

- Pointwise observations: refers to the analysis or measurement of a specific point within a dataset or mathematical function. In the context of functions, it pertains to properties or behavior at a single point.
- Localized observations: involve looking at the behavior or properties of a function or dataset within a small region surrounding a particular point. This is more about the vicinity of a point rather than just the point itself.

Before we delve into the analysis of these two cases, we need to make an additional assumption regarding the kernel of the history function. This assumption is based on our desire to minimize the impact of recent temperature data and focus more on temperatures from earlier historical periods. To achieve this, we specify the kernel in the following form:

$$\exists \epsilon > 0 \ \text{ such that } \ \kappa(s,\cdot) = 0, \quad [-\epsilon, 0]$$

Thus the history function becomes:

$$H(t,x,u) := \int_{-\tau}^{-\epsilon} \kappa(s,z) u(t+s,z)\, ds$$

For the next subsections we will assume that these conditions are satisfied.

5.2.1 Pointwise Observation

In order to get a uniqueness solution with sufficient regularity we will introduce the following sets:

- The set of **admissible Initial Conditions**:

$$N^{(pw)} := C^{1,2}([-\tau, 0] \times [-1, 1]) \tag{5.2.1}$$

- The set of **admissible coefficients**:

$$\mathcal{M}^{(pw)} := \{q \quad \text{is Lipschitz continuous and piecewise analytic on} \quad (-1, 1)\} \tag{5.2.2}$$

We can now present the uniqueness result of the Inverse Problem with Pointwise Observations.

Theorem 5 *Consider two different insolation functions $q, \tilde{q} \in \mathcal{M}^{(pw)}$ and assume the initial condition $u_0 = \tilde{u_0} \in N^{(pw)}$.*

Assume that $\exists z_0 \in (-1, 1)$ and $T > 0$ such that:

$$\forall t \in (0, T) \quad \begin{cases} u(t, z_0) = \tilde{u}(t, z_0) \\ u_x(t, z_0) = \tilde{u_x}(t, z_0) \end{cases}$$

Then the two insolation functions are identical, i.e., $q \equiv \tilde{q}$ on I.

Remark 7 *Theorem 5 establishes that the insolation function is uniquely determined within interval I by the measurements of u and u_x at a specific point z_0 over the time interval $(0, T)$. The diagram below illustrates the region sufficient to demonstrate the uniqueness of the insolation function.*

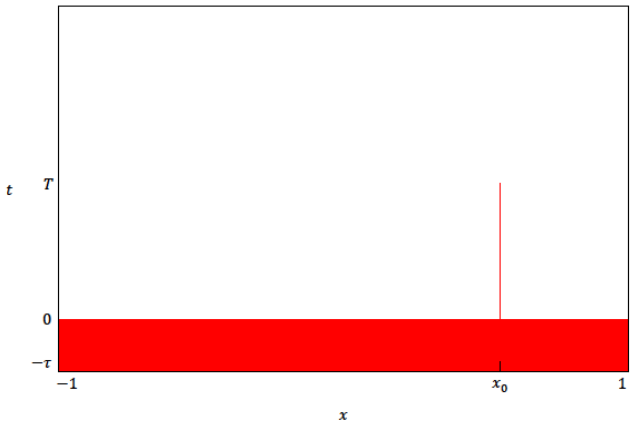

Figure 5.1: Space - time measurement region which can lead to unique coefficient determination for the case of Pointwise Observations(source [**9**])

5.2.2 Localized Observation

Following the procedure outlined in the previous subsection and ensuring sufficient regularity of the solution, we introduce two useful sets below.

- The set of **admissible Initial Conditions**, for:

$$D > 0 \quad N^{(loc)} := \{u_0 \in C([-\tau, 0]; Y \cap L^\infty(-1,1)),\ \ u_0(0) \in D(A),\ \ Au_0(0) \in L^\infty(I), \\ \sup_{t\in[-\tau,0]} \left(\|u_0(t)\|_Y + \|u_0(t)\|_{L^\infty}\right) + \|Au_0(0)\|_{L^{\infty(I)}} \leq D\}$$

- The set of **Admissible Coefficients**, for:

$$D' > 0 \ \ \mathcal{M}^{(loc)} := \{q \in L^\infty(I) : \|q\|_{L^{\infty(I)}} \leq D'\}$$

Now we are ready to present the Lipschitz stability Theorem.

Theorem 6 *Considering a middle time $0 < t < \epsilon'$. Choosing, $t_0 \in [0, t')$, and suitable $D, D' > 0$ then, $\exists B(t_0, T', T, D, D') > 0$ such that, for all $u_0, \tilde{u_0} \in N^{(loc)}$, $\forall q, \tilde{q} \in \mathcal{M}^{(loc)}$, the solutions $u, \tilde{u}$ of (2.3.3),satisfy:*

$$\|q - \tilde{q}\|^2_{L^2(I)} \leq B\Big(\|u(T') - \tilde{u}(T)\|^2_{D(A)} \\ + \|u_t - \tilde{u}_t\|^2_{L^2((t_0,T)\times(a,b))} + \|u_0 - \tilde{u}_0\|^2_{C([-\tau,0];Y)}\Big) \quad (5.2.3)$$

where $(a, b) \subset (-1, 1)$ an area around x_0.

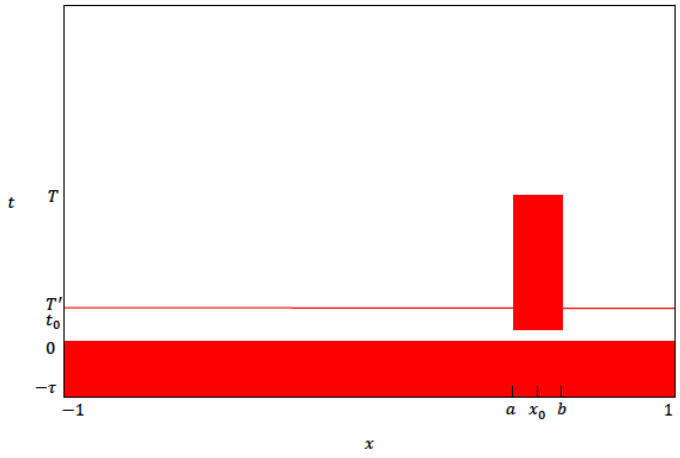

Figure 5.2: Space - time measurement region which can lead to unique coefficient determination for the case of Localized Observations(source [**9**])

Bibliography

[1] Hunter CM, Caswell H, Runge MC, Regehr EV, Amstrup SE, Stirling I, Climate change threatens polar bear populations: a stochastic demographic analysis, Ecology 2010, https://doi.org/10.1890/09-1641.1

[2] A. Bensoussan, G. Da Prato, M.C. Delfour, S.K. Mitter, Representation and Control of Infinite-Dimensional Systems, vol. 1, Systems Control Found. Appl., Birkhäuser Boston, Inc., Boston, MA, 1992

[3] G. Floridia, Nonnegative controllability for a class of nonlinear degenerate parabolic equations with application to climate science, Optimization and Control, 2020, https://doi.org/10.48550/arXiv.2003.04966

[4] Sellers W. D., A Global Climatic Model Based on the Energy Balance of the Earth-Atmosphere System, Institute of Atmospheric Physics, University of Arizona, Journey of Applied Meteorology, Volume 8, 1969

[5] Sellers W. D., The effect of changes in the earth's obliquity on the distribution of mean annual sea-level temperatures, J. Appl. Meteo- rol., 9, 960-961, 1970.

[6] G. R. NORTH, J. G. MENGEL, AND D. A. SHOR, Simple Energy Balance Model Resolving the Seasons and the Continents' Application to the Astronomical Theory of the Ice Ages, JOURNAL OF GEOPHYSICAL RESEARCH, VOL. 88, NO. C11, PAGES 6576-6586, AUGUST 20, 1983

[7] Ghil M. 1976 Climate stability for a Sellers-type model. J. Atmos. Sci. 33, 3–20. $(doi.org/10.1175/1520-0469(1976)033<0003:CSFAST>2.0.CO;2)$

[8] Ghil M., 1984, Climate sensitivity, energy balance models, and oscillatory climate models, Journal of Geophysical Research-Atmospheres,Volume89, Issue D1, doi.org/10.1029/JD089iD01p01280

[9] Bhattacharya K, Ghil M, Vulis IL. 1982 Internal variability of an energy-balance model with delayed albedo effects. J. Atmos. Sci. 39, 1747–1773. $(doi : 10.1175/1520-0469(1982)039<1747:IVOAEB>2.0.CO;2)$

[10] J. Tort, J. Vancostenoble, Determination of the insolation function in the nonlinear Sellers climate model, Ann. I. H. Poincaré – AN 29 (2012) 683–713

[11] P. Cannarsa, M. Malfitana, AND P. Martinez, Parameter Determination For Energy Balance Models with Memory,Springer INdAM Series, In press. ffhal-01834739, (2018)

[12] M. I. Budyko, The effect of solar radiation variations on the climate of the Earth, Main Geophysical Observatory, Leningrad, M. Spasskaja 7,Vol 21,Issue 5, (1969), doi.org/10.1111/j.2153-3490.1969.tb00466.x

[13] https://science.nasa.gov/science-research/earth-science/milankovitch-orbital-cycles-and-their-role-in-earths-climate/

[14] J. I. Diaz, On the mathematical treatment of energy balance climate models, NATO ASI Ser. Ser. I Glob. Environ. Change, 48, Springer, Berlin, 1997

[15] A. Bensoussan, G. Da Prato, M.C. Delfour, S.K. Mitter, Representation and Control of Infinite-Dimensional Systems, vol. 1, Systems Control Found. Appl., Birkhäuser Boston, Inc., Boston, MA, 1992.